PROCEEDINGS, 45th Workshop on Geothermal Reservoir Engineering
Stanford University, Stanford, California, February 10-12, 2020
SGP-TR-216

Use of Short-Wave Infrared Reflectance (SWIR) Spectroscopy to Characterize Hydrothermal alteration minerals in Olkaria Geothermal System, Kenya.

Mathew Kamau[1], Chris Hecker[2] and Caroline Lievens[2]

[1]Kenya Electricity Generating Company Limited P.O Box 785, 20117, Naivasha

[2]University of Twente, Faculty of Geo-Information Science and Observation (ITC), P.O Box 37, Enschede 7500 AA, Netherlands

mwkamau@kengen.co.ke, c.a.hecker@utwente.nl, c.lievens@utwente.nl

Keywords: Olkaria geothermal system, Hyperspectral Imaging, Infrared Spectroscopy, Hydrothermal alteration minerals

ABSTRACT

Hydrothermal minerals and mineral assemblages formed in a geothermal system provide information on both present and past geothermal reservoir conditions. Conventionally, identification and characterization of hydrothermal minerals in Olkaria geothermal system involves use of binocular microscopes, petrographic, fluid inclusion and XRD techniques. These methods though useful are time consuming and relatively expensive in terms of sample processing and analysis procedures. With high volume of samples being generated during geothermal drilling, a fast and cost-effective technique to map hydrothermal alteration minerals is required. Over time, Infrared spectroscopy has shown to be fast, cost-effective, non-destructive, reproducible and repeatable analytical technique. In this regard, this paper describes infrared spectroscopy technique and its potential to identify and characterize hydrothermal alteration minerals in a geothermal system. Particularly, it presents SWIR hyperspectral imaging results of three geothermal wells in Olkaria geothermal system. Hyperspectral images were acquired from drill cuttings samples using SWIR camera (Specim Ltd, Finland) located in the Geo-science Laboratory in the University of Twente ITC, Enschede, Netherlands. It had a pixel size of 260 µm and a spectral range of between 1000-2500 nm consisting of 288 spectral bands. Spectral identification was done by comparing mineral spectra with published spectra. Smectites, zeolites, illite, chlorite, calcite, epidote and amphiboles, were positively identified using this technique. Results were successfully used to interpret hydrothermal alteration minerals and mapping of alteration zones in each borehole studied. Lastly, information derived were used to decipher the location of borehole as either in-flow, out-flow or cold-influx zone which is critical information in borehole siting.

1. INTRODUCTION

Identification and interpretation of hydrothermal mineral assemblages is an important aspect of surface and sub-surface exploration of the geothermal resource (Milicich et al., 2015). They provide insight into the present and/or past nature of the geothermal reservoir. Conventionally, hydrothermal minerals are best identified by the aid of analytical techniques which encompass but not limited to the binocular microscope, petrographic microscope, scanning electron microscope and X-ray diffractometer (XRD) analyses. Most recently, Infrared reflectance(IR) spectroscopy is increasingly being used with varying levels of success as an exploration tool in the mining industry e.g Kruse, (1996) and to a lesser extent for geothermal exploration (Calvin & Pace, 2016). This technique rapidly collects mineralogical information particularly alteration minerals that are difficult to distinguish in hand sample, binocular or by petrographic methods (Calvin & Pace, 2016). It works by the acquisition of reflectance spectra within Visible Near Infrared(VNIR)-Short Wave Infrared (SWIR) with a wavelength range of between 350-2500 nm in the electromagnetic spectrum (Mathieu et al., 2017).

In Olkaria geothermal system, assessment of hydrothermal minerals largely utilizes analytical techniques such as binocular microscope, petrographic microscopes, scanning electron microscope and X-ray diffractometer (XRD). Considering the number of samples collected per well, these methods can be time consuming and relatively expensive in terms of sample processing and analysis procedures. Besides, consistent analysis of hydrothermal minerals during drilling of a geothermal well require implementation of an in situ, cost effective and quick analytical methods with comparable results from different operators. Moreover, data collected should be capable of being stored in accessible database for eventual interpretation. Over time, reflectance spectroscopy has proved to be fast, cost effective, non-destructive reproducible and repeatable analytical technique (Simpson, 2015). For instance, Simpson & Rae, (2018) successfully characterized clays minerals associated with geothermal system using point measurement by Analytical Spectral Device(ASD). However, this technique allows limited numbers of spectra to be produced per sample thus minimizing number of minerals that can be identified. In this paper, the study focuses on use of hyperspectral imaging technique to identify and characterize hydrothermal alteration minerals in Olkaria geothermal system. The technique combines both spectral and spatial imaging methods by acquiring images with a high number of contiguous spectra. This allows spectral analysis of each discrete pixel thus enabling new investigations and yield in a novel or unexpected mineralogical and petrological insight into variety of geological processes.

2. LOCATION AND GEOLOGY

2.1 Location

Olkaria geothermal field is in Kenyan Rift valley to the south of Lake Naivasha about 120 km NW of Nairobi. It is a high-temperature geothermal system with an approximate area of about 240 km^2. The geothermal system is associated with one of the several volcanic centers situated within the Kenyan Rift (Ofwona, 2002). It has been divided into seven sub-fields (Figure 1) with Olkaria Hill a prominent geological feature being the reference point (Otieno, 2016). Production in the field began in the early 1980s with installation

of 45 MWe power plant. To date, close to 300 geothermal wells have been drilled with a depth of between 1000-3600 m. The installed aggregate capacity of the field is estimated at 688 MWe.

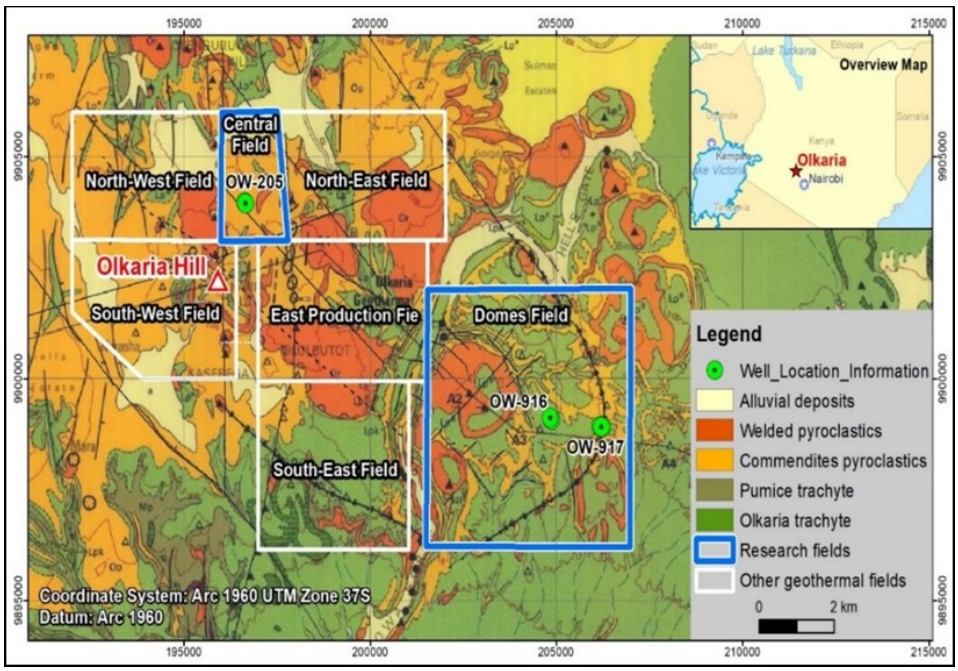

Figure 1: Showing surface geology and location of OW-205, OW-916 and OW-917. Overview map shows location of Olkaria geothermal system

2.2 Geology and geological setting

Olkaria geothermal system is inside a major volcanic complex that has been cut by a N-S trending normal rifting faults inside the Kenyan rift (Axelsson et al., 2013). Activities associated with it entails at least 80 smaller volcanic centers consisting of comendite or peralkaline rhyolites (Clarke &Woodhall; 1990). Most of these volcanic centers are structurally controlled and occur as either steep-sided domes form of lava and/or pyroclastic rock or as thick lava flows. The rocks within Olkaria geothermal systems are associated with Quaternary Volcanism (Omenda, 1998) and consist of mildly peralkaline silicic volcanic domes, lava flows and air fallen pumice and peripheral basalts (Lagat et al., 2005).

Detailed geological study resulted in the documentation of the sub-surface geology using drill cuttings and cores obtained from geothermal wells. For instance, study by Muchemi et al., (1987), described sub-surface geology of Olkaria as consisting thick volcanic pile of predominantly alkaline, silicic rocks and pyroclastic materials with minor basaltic intercalations. Additionally, Omenda (1998), showed sub-surface geology as consisting of six litho-stratigraphic units namely, Upper Olkaria volcanic, Olkaria basalts, Plateau trachyte's, Mau tuffs, Pre-Mau volcanic and the basement system.

3. INFRARED SPECTROSCOPY

Infrared spectroscopy involves the study of light as a function of the wavelength emitted, reflected or scattered after light interacts with solid, liquid or gas. Infrared wavelength range is considered a good mineral detection range because it allows a wide range of minerals to be identified. It extends from Visible and Near-Infrared (VNIR, 400-1000 nm), through the Short-Wave Infrared (SWIR, 1000-2500nm), Mid-Wave Infrared (MWIR, 3000-5000nm) to the Long-Wave Infrared (LWIR, 7000-1300 nm). In VNIR range, absorption process is due to electronic transition of the iron cations. This process characterizes presence of ferrous and ferric iron oxides (e.g. hematite, jarosite). On the other hand, SWIR spectroscopy involves the detection of the reflected energy modulated by molecular vibrations, rotational, bending and stretching of bonds within the 1000-2500 nm wavelength range (Clark, 1999). In this range, minerals groups such as phyllosilicates, sorosilicate's, inosilicates, carbonates and zeolites exhibit characteristic spectra with diagnostic absorption features of certain molecular groups (e.g. OH, H_2O and NH_4) and cation hydroxyl bonds (e.g. Al-OH, Fe-OH and Mg-OH) within the mineral crystal lattice (Hunt, 1977). In a near complete suite of mineral identification, LWIR allows identification of mineral groups such as tectosilicates (e.g. feldspars, quartz, albite), inosilicates (e.g. diopside, amphiboles), phosphates (e.g. apatite), sulphates (Kraal & Ayling, 2019). In SWIR spectroscopy, the energy of absorption corresponds to distinct energy levels and occur in well-defined wavelength positions (Hauff, 2008). Each molecular group has characteristics absorption features occurring at a specific wavelength range. For instance, Thompson et al., (1999), showed the occurrence of OH and H_2O features at 1400 and 1900 nm respectively. Equally, he demonstrated the occurrence of diagnostic features related to Al-OH, Fe-OH and Mg-OH at 2200 nm, 2250 nm and 2330 nm wavelength range respectively.

Application of laboratory-based SWIR hyperspectral imaging sensors allows surface scanning of samples hence enabling new investigations that yields novel or unexpected mineralogical and petrological insights (Thomas & Walter, 2002). Moreover, images acquired enables creation of high resolution mineral maps which can be used to determine relative proportions of mineral mixtures in rock samples (Zaini et al., 2014). The images allows spectral analysis of each discrete pixel which permits identification of mineral chemistries (Goetz et al., 1985).

4. DATASET AND METHODOLOGY

4.1 Dataset

Drill cuttings used for this study are from three wells located in two sub-fields. OW-205 is located in Olkaria central sub-field while both OW-916 and OW-917 are located in Olkaria domes sub-field. Auxiliary data used includes; temperature data, lithological data, XRD data and shapefiles for making map.

4.1 Methodology

SWIR measurements were done on a total of 135 drill cuttings rock samples collected from the three boreholes. Hyperspectral Imaging was done using SWIR camera (Specim ltd; Finland) located in the Geo-Science Laboratory in the University of Twente, ITC Enschede, Netherlands. Technical specifications of SWIR camera used for this study are shown in Table 1 below;

Table 1: Technical Specifications of SWIR camera.

Type of the stage	Lab stage
Spectral range (nm)	1000-2500
Distance of the sensor to sample (cm)	30
Pixel size(μm)	260
Image swath(mm)	98
Number of bands	288
Lens focal length(mm)	OLES30 (30 mm)
Spectral Sampling	5.6 nm
Spectral resolution FWHM	12nm

Images of samples were made by passing samples on a translation stage underneath a camera. Image cubes were constructed using the camera in a push-broom style. Measurement of a white reference standard plate with (99%) reflecting surface of the incident light and a dark reference surface were taken before the measurements were done for image calibration.

4.2 Image processing

Representative spectra Endmembers (EMs) of the hydrothermal minerals were collected in a spectral library. For that purpose, a wavelength mapping was done (Hecker et al., 2019; Ruitenbeek et al., 2014) to see spatial patterns and mineral variation in a sample. The resulting product is an image product in RGB transformation where the hue represents the wavelength position and intensity the depth of the absorption feature (van der Meer et al., 2018). Spectral EMs were manually collected from the image data itself and stored in a spectral library. The appropriate name of the spectral EMs was assigned by comparison to USGS and GMEX spectral analysis guide (Pontual et al., 2008). Continuum removal process to remove background noise and isolate particular absorption features for easier identification and analysis was performed(Fang et al., 2018). Relative abundances of the most dominant hydrothermal minerals were estimated by image classification using Spectral Angle Mapper (SAM) classification algorithm. This was performed on all images using a spectral subset of between 2100-2400 nm using image derived endmembers and threshold of 0.1 radian.

4.3 Validation by X-ray diffractometer (XRD)

Minerals identified by spectroscopy technique were validated using Bruker D2 Phaser diffractometer located at the Geoscience Laboratory of ITC, University of Twente. Five (5) representative rock samples to be analyzed by XRD were selected based on spectral measurement from different depths in all the three boreholes studied. Mineral identification was done by using an automatic search and scan or manually searching by mineral name in DIFFRAC. EVA version 3.1 software against an inbuilt reference mineral database. Several best match peaks were generated by the software, but the ultimate likely mineral was selected by the user.

5. RESULTS

5.1 Smectites

Montmorillonite and nontronite are the main smectite minerals identified in this study. They were mainly mapped in the upper alteration zones. Montmorillonite was identified by use of an intense water absorption feature between 1911-1917 nm wavelength range and a major but broad Al-OH band between 2214-2225 nm wavelength ranges (Figure 2). In this study, it was only identified in OW-916 at depth of between 30-500 m.

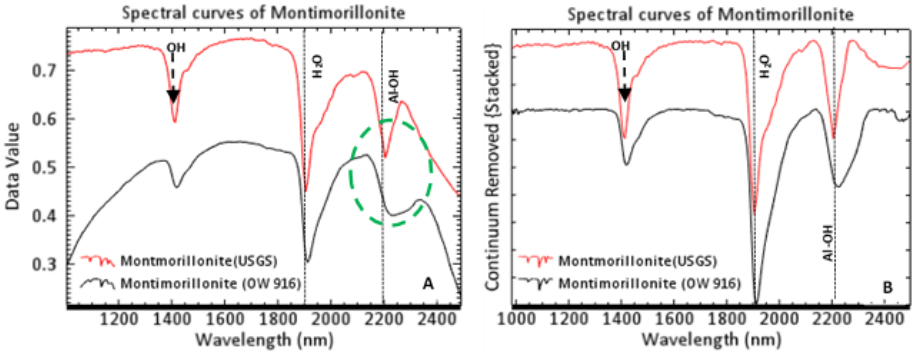

Figure 2: Spectral profiles (A) normal reflectance (B) continuum removed spectra of montmorillonite from OW-916 and USGS spectral library. Note the broad feature (circled) associated with montmorillonite spectra from the sample.

Nontronite is a di-octahedral smectite with a Fe^{2+} mineral. Compositionally, it consists of more than 30% Fe_2O_3 (Pontual et al., 2008). Analogous to montmorillonite, it is identified by the presence of deep H_2O absorption between 1911-1917 nm with iron diagnostic absorption feature occurring at between 2296-2298nm (Figure 3). It was identified in both OW-916 and OW-917.

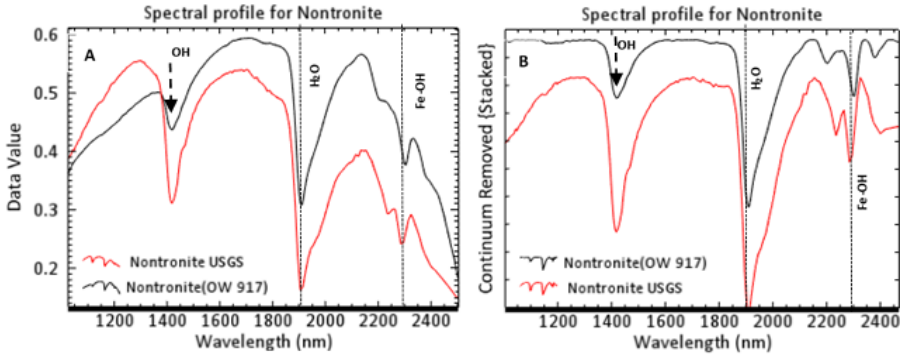

Figure 3: Spectral profiles (A) normal reflectance (B) Continuum removed spectra of Nontronite from OW-917 and USGS spectral library.

5.2 Zeolites

In a geothermal system, zeolites are commonly present in the upper part of the alteration sequence where temperature are $<120^0$C). The most commonly identified zeolite in this study is mordenite. Identified by intense water absorption feature near 1416 and 1911 nm wavelength range (Figure 4). It occurred in all the three well studied. It was distinguished from smectite due to lack of characteristic feature near 2200 nm. In OW-916, its appearance is from the first sample (20-30 m) to approximately 1000m. However, it was more intense and abundant between 30-450 m with a temperature of below 100^0C. In OW-917, mordenite appeared between the first sample (50-52 m) up to approximately 300 m. In OW-205, it first appeared from the first sample analyzed (512-514 m) up to approximately 1000 m with a measured formation temperature of $> 200^0$C.

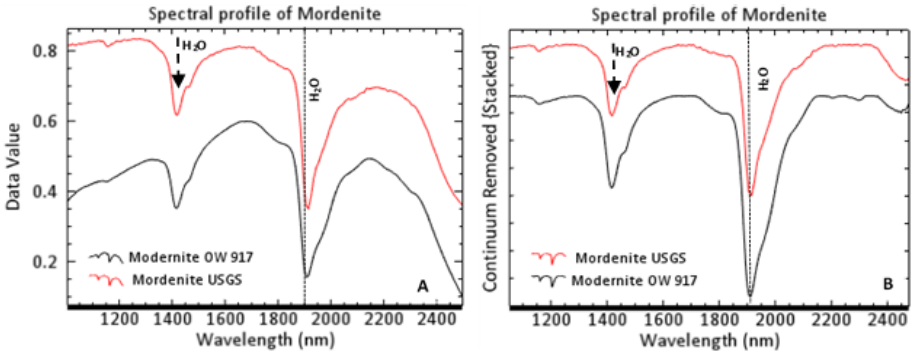

Figure 4: Spectral profile of (A) normal reflectance (B) continuum removed spectra of mordenite from OW-917 sample and USGS spectral library

5.3 Illite

It is a common hydrothermal mineral identified in the study area. It is identified by use of Al-OH absorption feature between 2197-2225 nm wavelength range (Figure 5). In OW-205, illite was identified in almost every sample analyzed cutting across all lithological units. Wavelength position of the absorption feature varied between 2199-2224 nm. In OW-916, it first appeared at approximately 500 m depth then appeared sporadically up to the bottom of the hole. Spectral characteristic features varied between 2198-2224 nm wavelength range. In OW-917, it first appeared at 1800 m depth and persisted downhole. Spectral features varied between 2213-2224 nm wavelength range.

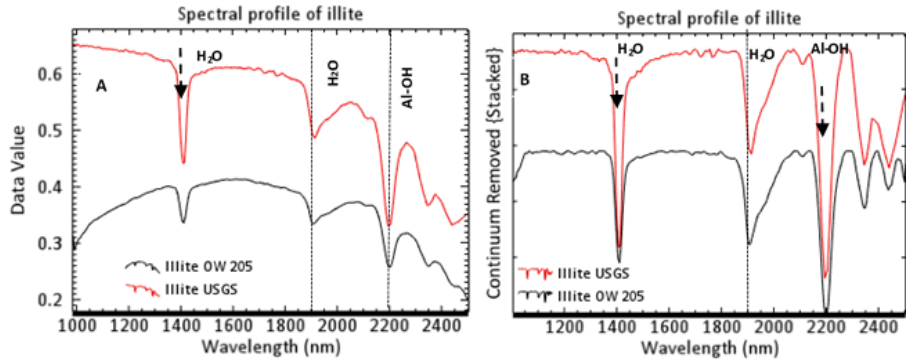

Figure 5: Spectral profile of (A) normal reflectance of illite (B) Continuum removed of spectra from USGS spectral library and OW-205

5.4 Chlorite

It was spectrally identified by use of Fe-OH feature between 2245-2262 nm wavelength range (Figure 6). It commonly occurred in mixture with illite where Fe-OH feature was largely obscured by spectrally dominant Al-OH feature. In OW-205, it was generally present in all samples analyzed. In OW-916, chlorite first appeared at approximately 400 m depth with irregular appearance observed with increase in depth while in OW-917, it first appeared in trace amount near 500 m depth and only re-appeared again below 1500 m depth.

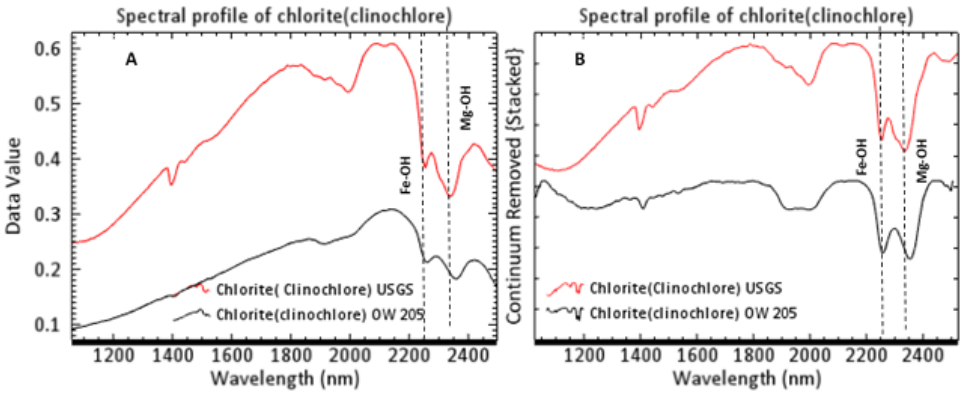

Figure 6: Spectral profile of (A) normal reflectance (B) Continuum removed spectra of chlorite from OW-205 and USGS spectral library.

5.5 Epidote

It is a common hydrothermal mineral found in the study area. Spectrally, it was identified by use of absorption feature near 1540 nm, Fe-OH diagnostic feature located near 2256 nm and Mg-OH feature between 2335-2342 nm wavelength range (Figure 7). Primarily, it occurred in mixture with chlorites, carbonates and amphiboles. In OW-205, epidote first appeared near 1050 m and persisted downhole. It occurred together with illite, chlorite, calcite and amphiboles in almost all the depth it was recognized. In OW-916, it was first appeared spectrally at 1300 m and then appeared sporadically to the bottom of the hole. In OW-917, epidote appeared in trace amount starting from 1850 m. It occurred in association with illite, chlorite calcite and amphibole.

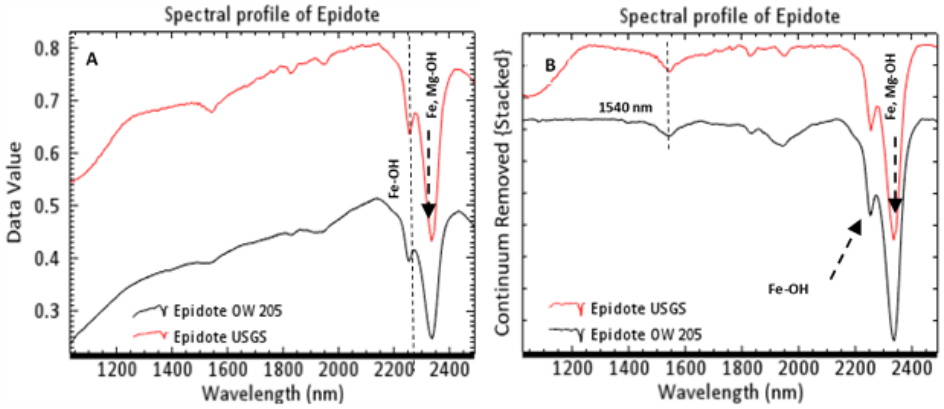

Figure 7: Spectral profile of (A) normal reflectance (B) Continuum removed spectra of epidote from OW-205 and USGS spectral library.

5.6 Amphiboles

Two amphibole minerals were spectrally identified from the study area namely actinolite and hornblende. Identification was by use of Mg-OH characteristic feature which varied between 2314-2324 nm and 2326-2350 nm for actinolite and hornblende respectively (Figure 8). In this case, hornblende occurs at a longer wavelength compared to actinolite. It was more abundant in OW-205 compared to OW-916 and OW-917. In OW-205, the first appearance of amphibole was at 900 m depth and its presence persisted downhole. In OW-916, it first appeared at 1300 m depth in assemblage with illite, chlorite and epidote. Most conspicuous, is the appearance of amphibole at shallow depth (600 m) in OW-917. However, its presence in this well disappeared with an increase in depth.

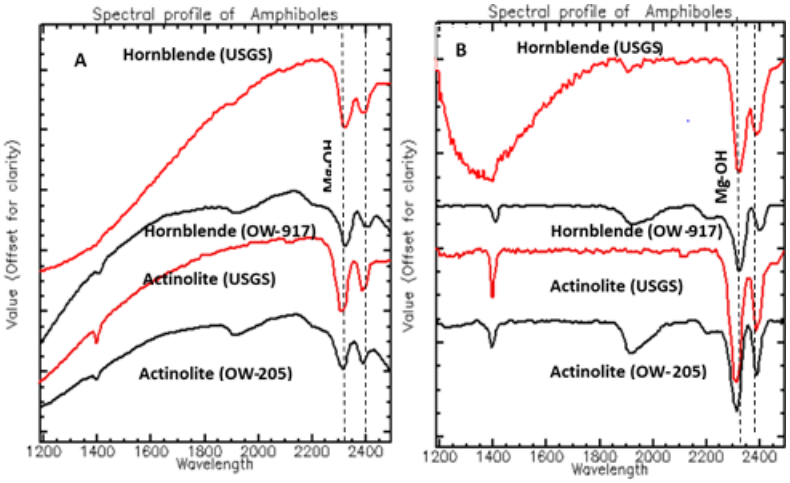

Figure 8: Spectral profile actinolite and hornblende minerals from USGS library and OW-205 & OW-917 (A) Normal reflectance (B) continuum removed spectra. Arrows shows shift in Mg-OH from shorter wavelength to longer wavelength from actinolite to hornblende.

5.7 Carbonate

Calcite is the most common identified carbonate mineral in the study area. The main diagnostic feature was by use of CO_3 characteristics feature occurring between 2340-2345 nm wavelength range (Figure 9). In this study, its spectral feature overlaps with those of chlorite, epidote and amphibole. Nevertheless, use of unique features in other minerals e.g. 1540 nm feature of epidote was used to distinguish them. In OW-205, calcite occur from 700 m downhole in association with chlorite, epidote and amphibole. Conversely, in OW-916, it appears in a localised zone between 500-1400 m depth where it is in association with illite, chlorite and epidote and in some cases amphibole. In OW-917, it occurred from 500 m down hole appearing in trace amount below 2600 m depth.

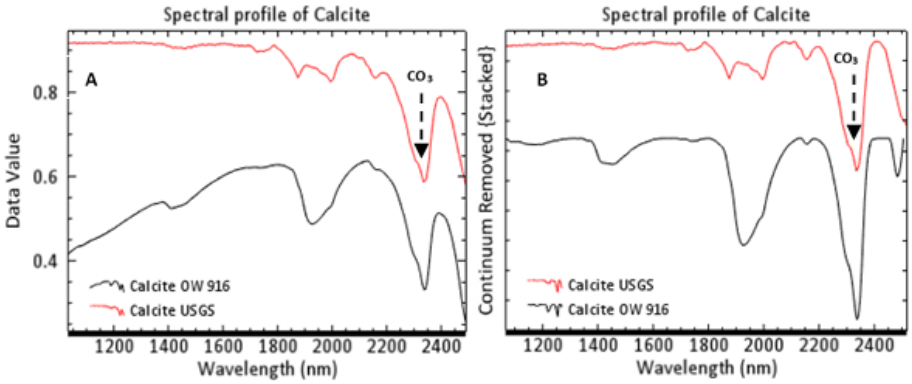

Figure 9: Spectral profile of (A) normal reflectance (B) Continuum removed spectra of calcite from OW-916 and USGS spectral library.

5.8 Spectral mixtures

Commonly identified spectral mixture in this study are illite-chlorite, chlorite-epidote and chlorite-calcite mineral mixtures. Illite-chlorite spectral mixture was indicated by a weak inflection on Al-OH feature by Fe-OH feature near 2240 nm wavelength range as shown in Figure 10.

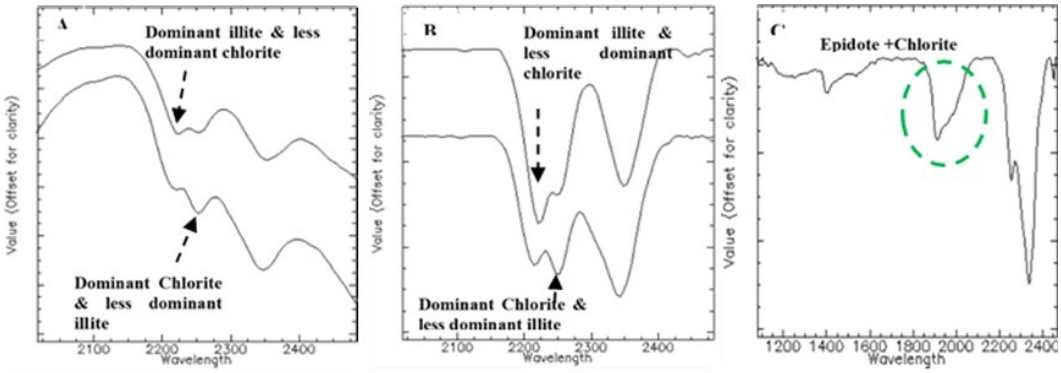

Figure 10: Spectral profile of mixed spectra of dominant illite& less dominant chlorite and dominant chlorite & less dominant illite (A) Normal reflectance (B) continuum removed (C) Spectra mixture of epidote +Chlorite. Note the broad feature (circled) associated with epidote+chlorite mixture.

5.9 Wavelength mapping

Results is shown by various stretches applied on the image in order to distinguish different group of minerals. For illustration, Figure 11 is a wavelength stretch 2300-2370 nm targeting Mg-OH group of minerals for sample OW-205 (2066-2070 m) depth. Yellow pixels (2337-2342 nm) corresponds to epidote minerals which is the dominant mineral in this sample. Cyan color pixels (2314-2320 nm) correspond to actinolite minerals while reddish pixels (2354-2362 nm) corresponds to Mg-OH feature of chlorite mineral.

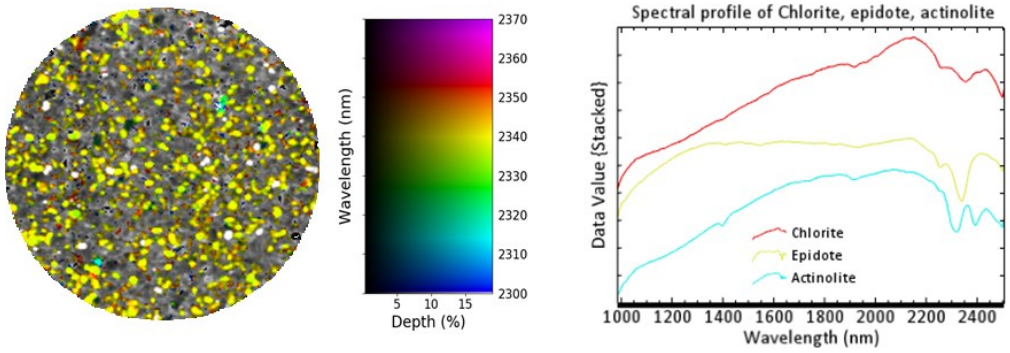

Figure 11: Wavelength map for the wavelength range 2300-2370 m for sample number OW-205(2066-2070 nm) and the spectra derived from the image.

5.10 Spectral Angle Mapper Classification

Classification results were based on the most dominant mineral species in each pixel where each pixel represent one mineral species. For illustration, Figure 12 show classification results of an upper alteration sequence of OW-916 sample OW-916(498-500 m). Chlorite and illite-chlorite mixture are the most predominant minerals in this sample.

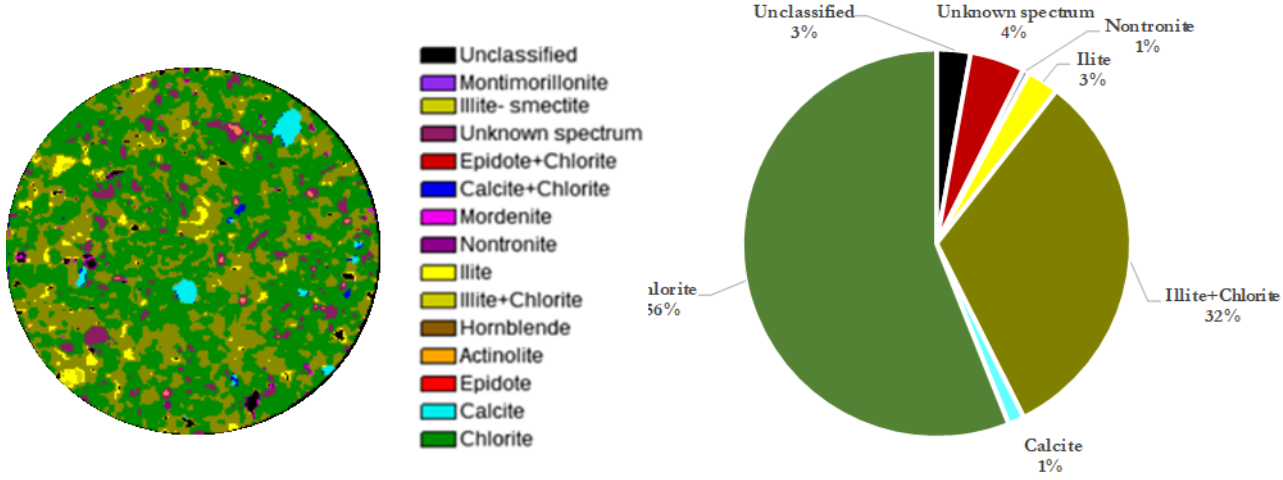

Figure 12: Classified image of sample OW-916 (498-500 m) using Spectral Angle Mapper and relative abundance of dominant minerals.

5.11 Results validation by XRD

Figure 13 shows diffractograms of minerals identified by XRD technique in sample OW-916(498-500m) depth.

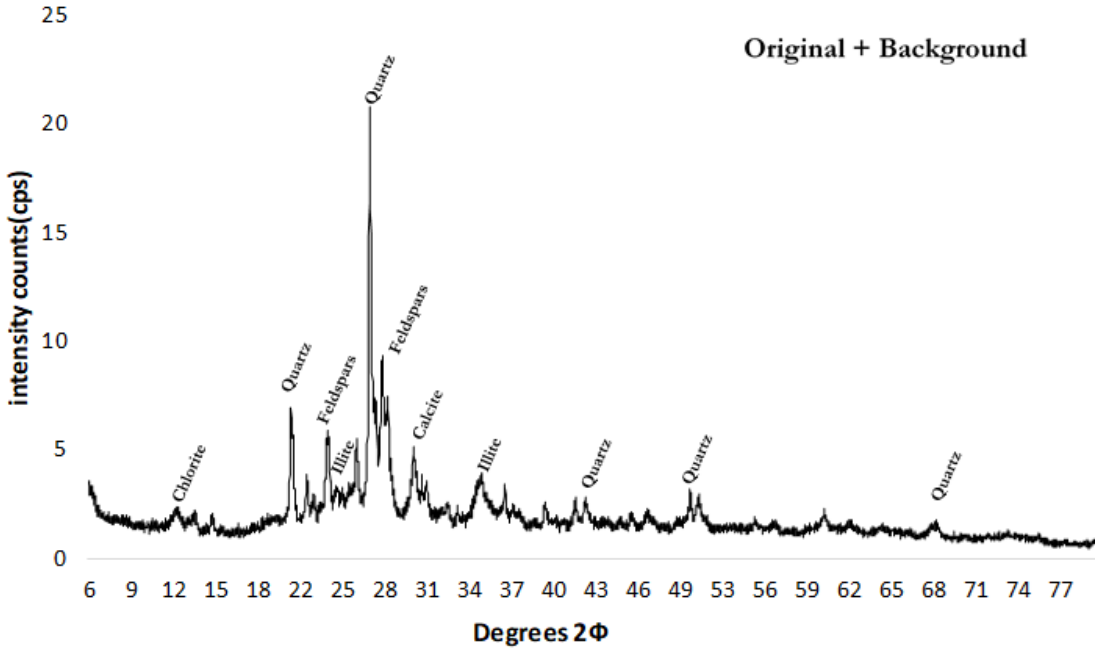

Figure 13: Representative XRD pattern of sample OW-916(498-500 m) showing peaks of illite, chlorite, quartz, illite and feldspars. Illite and chlorite hydrothermal minerals were earlier identified in SWIR as shown in Figure Error! Reference source not found. **15.**

6. DISCUSSION

6.1. Data Integration

A comparison of lithology, temperature, alteration mineralogy, spectral parameters of illite and chlorite mineral, relative mineral abundance derived from SAM classification and the alteration zones were plotted together on each well as illustrated by Figure 14-16

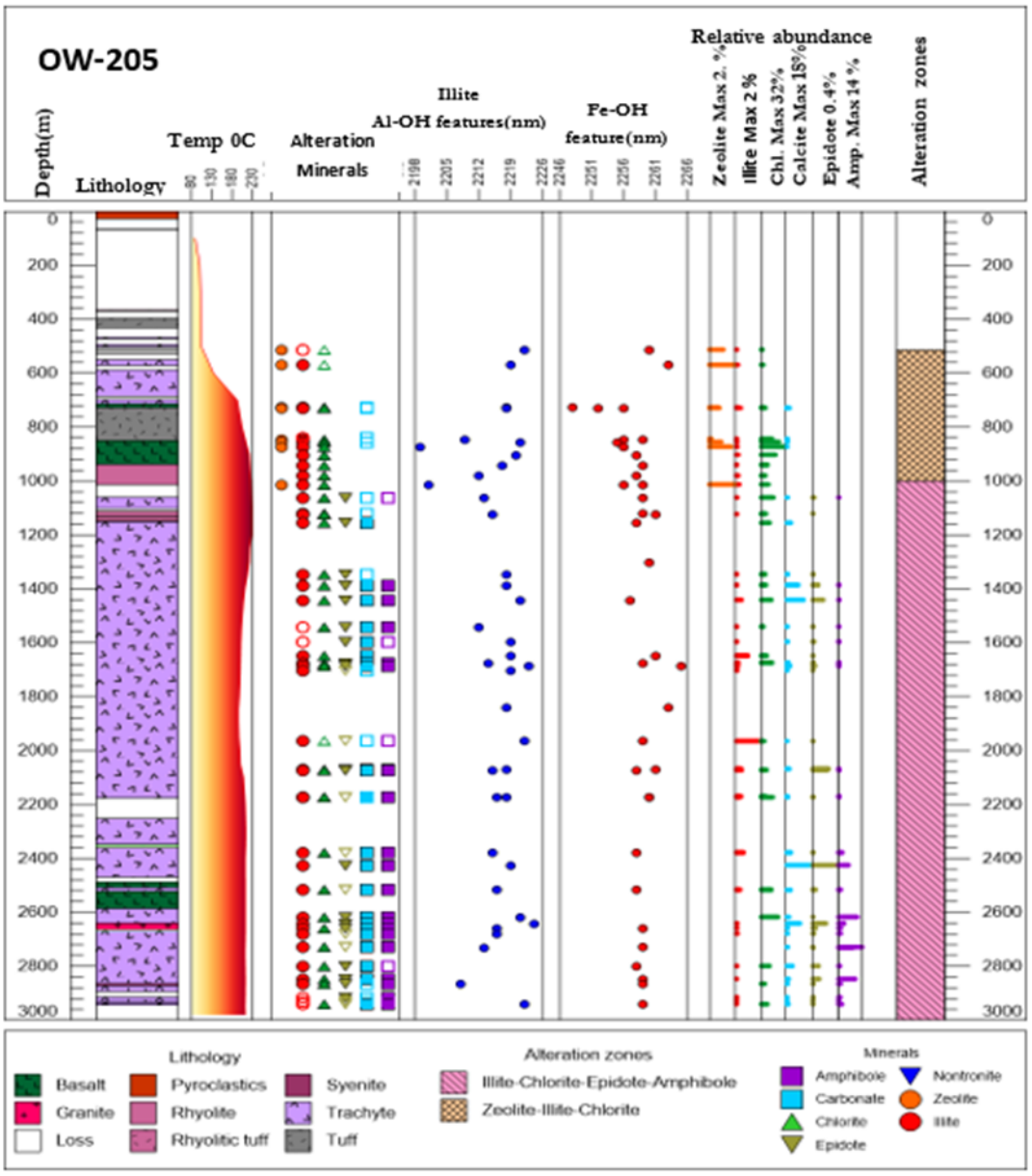

Figure 14:SWIR identified hydrothermal minerals and spectral parameters plots for illite, and chlorite compared against lithology, measured well temperature, relative abundances and the alteration zone for OW-205. The filled mineral symbols represent minerals that were abundantly identified while the open one represents trace amount. The maximum relative abundance obtained for each mineral is indicated alongside mineral in the mineral column. Temperature and stratigraphic data used for this well was supplied by KenGen.

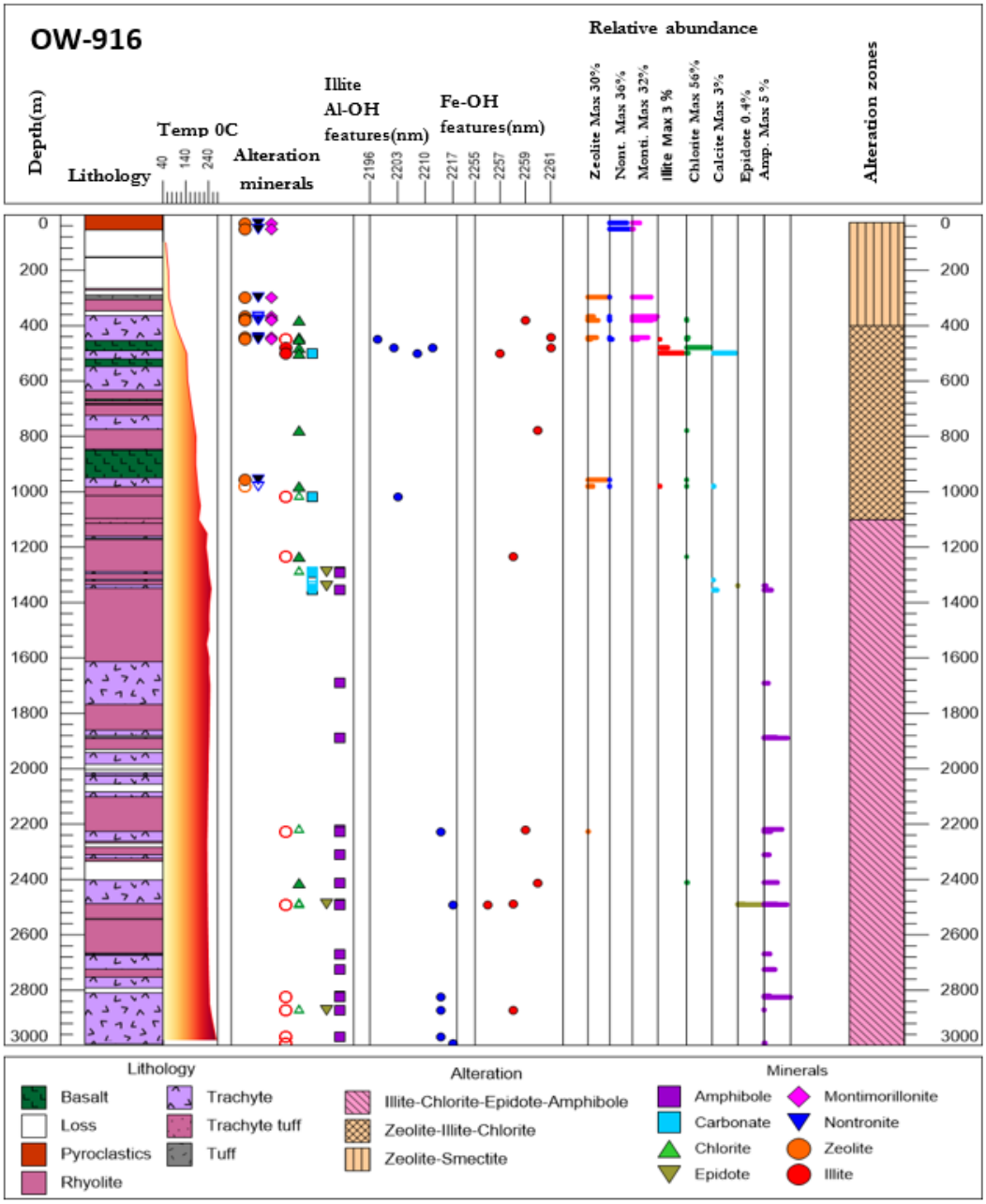

Figure 15:SWIR identified hydrothermal minerals and spectral parameters plots for illite and chlorite compared against lithology, measured well temperature, relative abundances and the alteration zone for OW-916 an up-flow well. The filled mineral symbols represent minerals that was abundantly identified while the open one represents trace amount. Temperature and stratigraphic data used for this well supplied by KenGen.

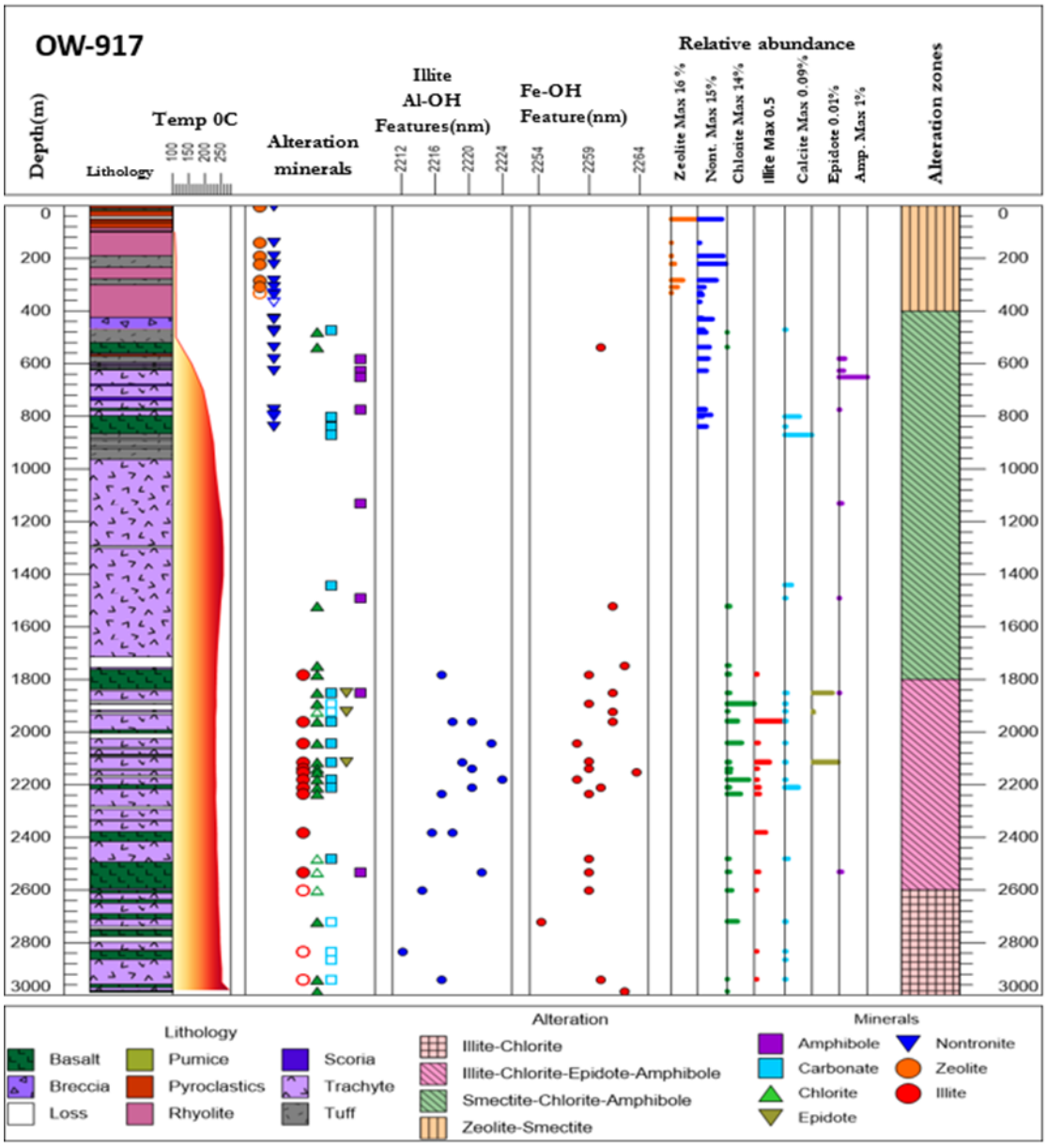

Figure 16:SWIR identified hydrothermal minerals and spectral parameters plots for illite and chlorite compared against lithology, measured well temperature, relative abundances and the alteration zone for OW-917 an up-flow well. The filled mineral symbols represent minerals that was abundantly identified while the open one represents trace amount. Temperature and stratigraphic data used for this well supplied by KenGen.

6.2. Hydrothermal alteration

The main alteration zones revealed in this study are illite-chlorite-epidote-amphibole zone, zeolite-illite-chlorite zone, illite-chlorite zone, smectite-chlorite-amphibole zone and zeolite-smectite zone. Illite-chlorite-epidote-amphibole zone is found in all the three wells studied. In OW-205, it is primarily found in trachytic rocks while in OW-916 and OW-917, it is found in trachytic-rhyolitic intercalation and basaltic-tuffaceous rock materials respectively. Zeolite-illite-chlorite zone is found in OW-205 and OW-916. In OW-205, is primarily found in basaltic and tuffaceous rocks while in OW-916, is found in intercalation of basalt, trachyte and trachytic tuff. In OW-916 and OW-917, zeolite-smectite zone is primarily found in the upper alteration sequence containing rhyolitic materials. Notably, is the absence of this zone in OW-205 probably because of absence of spectral data due to lack of drill cuttings at these depths. Smectite-chlorite-amphibole zone and zeolite-smectite zone in OW-917 is primarily found in trachyte-tuff-basalt intercalation and trachyte-basalt intercalation respectively.

Distribution of clay minerals in the three wells studied shows temperature as the main factor controlling their formation. In OW-205, occurrence of zeolites up to relatively deeper depth (Figure 14) is attributed to low temperature in this well. The apparent occurrence of zeolite at 1000 m with measured formation temperature of above 230^0C is interpreted as wairakite, a calcium-rich zeolite formed in an

active hydrothermal system with stability temperature of above 200 ^{0}C (Browne, 1978). Earlier studies by Yang et al. (2001), described mordenite and wairakite as having similar spectral characteristics making it difficult to distinguish them spectrally. In this case, differences in stability temperature of mordenite and wairakite was applied to distinguish the two minerals. Illite-chlorite occur intermixed from 500 m depth downhole. Occurrence of illite at temperature above 180 ^{0}C temperature confirms earlier studies by Browne, (2000) which indicated stability range of illlite being above 180 ^{0}C. Presence of epidote and amphibole mineral between 1500-2200 m depth with measured formation temperature <200 ^{0}C (Figure 14), is perhaps the biggest temperature anomaly encountered in this study. With stability range of epidote and amphibole being >220 ^{0}C, their presence at this depth could be interpreted as being relict and does not reflect the prevailing thermal conditions. Therefore, these minerals were formed when the temperature was higher and hence the system could be experiencing temperature reversals due to the cooling effect from cold water incursion. Occurrence pattern of calcite in OW-205 has been recognized by previous studies (e.g Simmons & Christenson, 1993) and is attributed to the formation of calcite by replacement of rock-forming minerals through hydrolysis due to boiling liquid containing CO_2 gas. Based on this alteration pattern, OW-205 was interpreted as either cooling or being located in zone of cold water incursion.

Hydrothermal alteration and mineral assemblages observed in well OW-916 (Figure 15) are largely in equilibrium with the measured formation temperature. In this case, minerals display a prograde pattern of alteration where low-temperature minerals (e.g. zeolite-smectite) form at shallow depth and high-temperature minerals (e.g. epidote, amphibole) form at deeper levels. High abundance of smectite derived from spectral data at a shallower depth (< 450 m) can be interpreted as the clay cap which is an impermeable layer formed by upwelling of geothermal fluids from depths. The appearance of epidote and amphibole at around 1350 m depth at measured formation temperature >200 ^{0}C corresponds to its lower stability limit (Bird, 1983). Illite occur sporadically and in trace amount downhole. Based on the hydrothermal alteration pattern observed in OW-916, it is interpreted as an up-flow well.

In OW-917, formation of hydrothermal minerals shows a retrograde alteration pattern. As illustrated in Figure 16, hydrothermal mineral assemblages formed shows temperature reversal where high temperature minerals are found at much shallower depth and vice versa. For instance, sporadic appearance of amphibole with depth and its eventual disappearance from 2600 m depth is interpreted as due to decrease in temperature below their formation temperature. Appearance of amphibole at a shallower depth(600m) is probably due to high temperature at shallow depth associated with out-flow wells. Equally, formation of zeolite-smectite zone in the same well at deeper depth is inferred as due to low temperature at depth commonly found in out-flow wells. Based on this, OW-917 is interpreted as an out-flow well. Appearance of illite at deeper depth (1700-2200 m) is interpreted as due to improved permeability associated with close lithological boundaries of trachytic and basaltic rock intercalations observed in this region coupled with temperature above 180 ^{0}C. Largely, spectral measurement in this borehole shows scarcity of alteration mineral active in SWIR region despite high measured formation temperature (>200 ^{0}C) experienced. This is interpreted as due to low permeability and lack of sub-surface faults and fracture which allows hydrothermal fluids flow.

6.3. Composition variation of illite and chlorite

Variation in wavelength position of Al-OH feature in illite has been used to effectively estimate the chemical composition of illite in hydrothermal system (Yang et al., 2011). In this study, composition variation of illite is interpreted based on earlier studies by Yang et al. (2001) which indicated white mica with Al-OH absorption feature position of <2200 nm as muscovite and those > 2210 nm as phengite. In OW-205 and OW-916, wavelength position of the diagnostic feature ranges between 2198-2224 nm at shallow depth and shift to > 2210 nm at deeper depth. In OW-917, diagnostic absorption features of illite occurs above 2210 nm. Consequently, illite in OW-205 and 916 was is interpreted as muscovite-phengite mixture at shallow depth and phengite at deeper depth while in OW-917 as predominantly phengite.

Previously, spectral variation of Fe-OH feature in chlorite has been used as a tool to estimate chlorite composition. For instance, Pontual et al., (1997) demonstrated use of wavelength position of either or both Fe-OH and Mg-OH feature to estimate chlorite composition and that variation of the absorption feature is a function of Fe:Mg ratio. Most recently, Simpon and Rae (2018) used Fe-OH feature of chlorite to distinguish Fe-rich chlorite, Fe-Mg chlorite and Mg-rich chlorite. In this case, Mg-rich chlorite occurred between 2240-2249 nm, Fe-Mg chlorite between 2250-2256 nm and Fe-chlorite between 2257-2265 nm wavelength range. In this study, spectral data was used to estimate composition variation of chlorite in the three geothermal wells studied. In OW-205, wavelength position of the diagnostic feature of chlorite varied between 2246-2256 nm at shallow depth and between 2256-2265 nm at deeper depth whereas in OW-916 and OW-917 Fe-OH it varied between 2254-2265 nm wavelength range. Consequently, chlorite chemistry is interpreted as Fe-Mg chlorite at shallow depth in OW-205 and Fe rich chlorite at deeper depth of OW-205. Likewise, in OW-916 and OW-917, it was identified as predominantly Fe-rich chlorite. Generally, composition variation of chlorite resulting from the three wells appears to be controlled mainly by chemistry of the parental rock and fluid composition.

6.4. Comparison with XRD results

Most of the hydrothermal minerals (e.g. illite, chlorite, calcite, nontronite, epidote, amphibole) were identified in both SWIR hyperspectral imaging and XRD techniques. Most notably, is identification of high proportion of quartz and feldspars which are inactive in SWIR spectroscopy. Minimal sample preparation and analysis required in SWIR hyperspectral imaging technique allows a greater number of samples to be analyzed per well as compared with XRD technique. This gives spectroscopy an advantage by allowing higher spatial resolution of samples per well.

6. CONCLUSION

SWIR hyperspectral imaging has proved to be a powerful tool for identifying and characterizing hydrothermal alteration minerals formed in a geothermal system. Wide range of hydrothermal alteration minerals were identified using SWIR reflectance spectroscopy.

Zeolites, smectites, illite, calcite, chlorite, epidote and amphiboles were found to be the most common hydrothermal alteration mineral in the three wells studied. Hydrothermal alteration minerals and mineral assemblages identified spectrally in this study shows different alteration pattern in each well. In OW 205, two alteration zones were identified which includes, illite-chlorite-epidote-amphibole zone and zeolite-illite-chlorite zone. In OW-916, three alteration zones i.e. illite-chlorite-epidote-amphibole, zeolite-illite-chlorite and zeolite-chlorite zone were identified whilst in OW-917, four alteration zones were identified i.e. zeolite-smectite, smectite-chlorite-amphibole, illite-chlorite-epidote-amphibole and illite-chlorite zones. Distribution of these alteration zones is largely attributed to temperature variation in each well. In addition, the technique was able to estimate relative abundances of common hydrothermal minerals identified and distinguish mineral species found illite and chlorite minerals. Relative abundance estimated spectrally can be used to offer immediate practical application during the drilling process. For instance, abundance of smectite (swelling clays) at shallow depth can be used to anticipate possibility of having a stuck drill string. Equally, abundance of high temperature minerals e.g. epidote can be used to determine the appropriate casing depth. To identify and characterize all important mineral formed in a geothermal system, the study recommend use of full electromagnetic spectrum range in future spectroscopic studies. In this case minerals active in VNIR (e.g. goethite, hematite and jarosite), SWIR (e.g. sericite, pyrophyllite, chlorite, calcite, amphiboles) and LWIR (e.g. quartz, plagioclase, adularia, albite) regions can be identified.

ACKNOWLEDGEMENT

We would like to thank KenGen for providing access to drill cuttings, lithological data, reservoir data used for this study. Many thanks to NUFFIC Fellowship Programme (NFP) for making this research possible. Much appreciation goes to staff of University of Twente faculty of ITC and Geoscience laboratory for their assistance in acquiring hyperspectral images and advice.

REFERENCES

Axelsson, G., Arnaldsson, A., Ármannsson, H., Árnason, K., & Einarsson, G. (2013). Updated conceptual model and capacity estimates for the Greater Olkaria Geothermal System, Kenya. In *Workshop on Geothermal Reservoir Engineering*. Stanford, California: Stanford University. Retrieved from https://pangea.stanford.edu/ERE/pdf/IGAstandard/SGW/2013/Axelsson.pdf

Bird, D. (1983). *Calc-silicate mineralization in active geothermal systems*. Stanford, California.

Browne, P. R. L. (1978). Hydrothermal Alteration in Active Geothermal Fields. *Annual Review of Earth and Planetary Sciences*, *6*(1), 229–248. https://doi.org/10.1146/annurev.ea.06.050178.001305

Browne, P. R. L. (2000). Relationship between illite crystallinity and temperature in active geothermal systems of New Zealand. *Clays and Clay Minerals*, *48*(1), 139–144. https://doi.org/10.1346/CCMN.2000.0480117

Calvin, W. M., & Pace, E. L. (2016). Mapping alteration in geothermal drill core using a field portable spectroradiometer. *Geothermics*, *61*, 12–23. https://doi.org/10.1016/j.geothermics.2016.01.005

Clark, R. N. (1999). Spectroscopy of rocks and minerals, and principles of spectroscopy. *Remote Sensing for the Earth Sciences: Manual of Remote Sensing*, *3*, 3–58. https://doi.org/10.1111/j.1945-5100.2004.tb00079.x

Clarke, Woodhall, A. & D. (1990). *Geological, volcanological and hydrogeological controls on the occurrence of geothermal activity sorrounding Lake Naivasha, Kenya*. Nairobi.

Fang, Q., Hong, H., Zhao, L., Kukolich, S., Yin, K., & Wang, C. (2018). Visible and Near-Infrared Reflectance Spectroscopy for Investigating Soil Mineralogy: A Review. *Journal of Spectroscopy*, *2018*. https://doi.org/10.1155/2018/3168974

Goetz A.F.H, Vane.G, Solomon J.E, Rock B, N. (1985). Imaging Spectrometry for Earth Remote Sensing, *228*(4704), 1147–1153. Retrieved from https://repository.library.brown.edu/storage/bdr:419459/PDF/

Hauff, P. (2008). An overview of VIS-NIR-SWIR field spectroscopy as applied to precious metals exploration. *Arvada, Colorado: Spectral International Inc*, (January).

Hecker, C., van Ruitenbeek, F. J. A., van der Werff, H. M. A., Bakker, W. H., Hewson, R. D., & van der Meer, F. D. (2019). Spectral Absorption Feature Analysis for Finding Ore: A Tutorial on Using the Method in Geological Remote Sensing. *IEEE Geoscience and Remote Sensing Magazine*, *7*(2), 51–71. https://doi.org/10.1109/MGRS.2019.2899193

Hunt, G. R. (1977). Spectral signatures of particulate minerals in the visible and near infrared. *Geophysics*, *42*(3). https://doi.org/10.1190/1.1440721

Kraal, K. O., & Ayling, B. (2019). Hyperspectral Characterization of Fallon FORGE Well 21-31 : New Data and Technology Applications, (2016), 1–15.

Kruse, F. A. (1996). Identification and mapping of minerals in drill core using hyperspectral image analysis of infrared reflectance spectra. *International Journal of Remote Sensing*, *17*(9). https://doi.org/10.1080/01431169608948728

Lagat, J., Arnorsson, S., & Franzson, H. (2005). Geology, hydrothermal alteration and fluid inclusion studies of Olkaria domes geothermal field , Kenya. In *Proceedings, World Geothermal Congress 2005, Antalya, Turkey* (pp. 24–29). Antalya,Turkey. Retrieved from https://www.geothermal-energy.org/pdf/IGAstandard/WGC/2005/0649.pdf

Mathieu, M., Roy, R., Launeau, P., Cathelineau, M., & Quirt, D. (2017). Alteration mapping on drill cores using a HySpex SWIR-320m

hyperspectral camera: Application to the exploration of an unconformity-related uranium deposit (Saskatchewan, Canada). *Journal of Geochemical Exploration*, *172*, 71–88. https://doi.org/10.1016/j.gexplo.2016.09.008

Milicich, S. D., Chambefort, I., & Bignall, G. (2015). Hydrothermal Alteration : Separating Fact from Hyperbole. In *Proceedings World Geothermal Congress 2015, Melbourne, Australia, 19-25 April 2015*. Melbourne, Australia.

Muchemi, T. M. L., & G.G. (1987). Geology and Hydrothermal Alteration of the North and West exploration wells in Olkaria, Kenya. In *Proceeding 9th NZ Geothermal Workshop* (Vol. 82).

Ofwona. (2002). *A Reservoir Study of Olkaria East Geothermal System, Kenya*. United Nations University. Retrieved from https://orkustofnun.is/gogn/unu-gtp-report/UNU-GTP-2002-01.pdf

Omenda, P. A. (1998). The geology and structural controls of the Olkaria geothermal system, Kenya. *Geothermics*, *27*(1), 55–74. https://doi.org/10.1016/S0375-6505(97)00028-X

Otieno, V. O. (2016). *Borehole Geology and sub-surface petrochemistry of the Domes area , Olkaria geothermal field , Kenya , in relation to well OW-922*. United Nations University.

Pontual, S., Merry, N., & Gamson, P. (2008). GMEX1-Spectral Interpretation Field Manual.pdf. AusSpec International Pty. Ltd.

Pontual, S., Merry, N., & Gamson, P. (1997). Spectral Analysis Guides for Mineral Exploration: Vol 1 - Spectral Interpretation Field Manual. *AusSpec International Pty.* AusSpec International Pty. Ltd.

Rae, S. &. (2018). Short-wave infrared (SWIR) reflectance spectrometric characterisation of clays from geothermal systems of the Taupō Volcanic Zone, New Zealand. *Geothermics*, *73*(February), 74–90. https://doi.org/10.1016/j.geothermics.2018.01.006

Ruitenbeek, F. J. A. Van, Bakker, W. H., Werff, H. M. A. Van Der, Zegers, T. E., Oosthoek, J. H. P., Omer, Z. A., … Meer, F. D. Van Der. (2014). Mapping the wavelength position of deepest absorption features to explore mineral diversity in hyperspectral images. *Planetary and Space Science*, *101*, 108–117. https://doi.org/10.1016/j.pss.2014.06.009

Simmons, C. . (1993). Towards a Unified Theory on Calcite Formation in Boiling Geothermal Systems (pp. 145–148). Retrieved from https://www.geothermal-energy.org/pdf/IGAstandard/NZGW/1993/Simmons.pdf

Simpson, M. P. (2015). Reflectance spectrometry [SWIR] of alteration minerals surrounding the Favona epithermal vein. Waihi vein system, Hauraki Goldfield. *AusIMM New Zealand Branch Annual Conference 2015*, (August 2015), 490–499.

Simpson, M. P., & Rae, A. J. (2018). Short-wave infrared (SWIR) Reflectance spectrometric characterisation of clays from geothermal systems of the Taupō Volcanic Zone, New Zealand. *Geothermics*, *73*(October 2017), 74–90. https://doi.org/10.1016/j.geothermics.2018.01.006

Thomas, M., & Walter, M. R. (2002). Application of hyperspectral infrared analysis of hydrothermal alteration on Earth and Mars. *Astrobiology*, *2*(3), 335–351. https://doi.org/10.1089/153110702762027916

Thompson J.B.; Hauff Phoebe L.; (1999). Alteration mapping in exploration; application of short-wave infrared SWIR spectroscopy. *SEG Newsletter*. Retrieved from https://eurekamag.com/research/029/972/029972329.php

Van der Meer, F., Kopačková, V., Koucká, L., van der Werff, H. M. A., van Ruitenbeek, F. J. A., & Bakker, W. H. (2018). Wavelength feature mapping as a proxy to mineral chemistry for investigating geologic systems: An example from the Rodalquilar epithermal system. *International Journal of Applied Earth Observation and Geoinformation*, *64*, 237–248. https://doi.org/10.1016/J.JAG.2017.09.008

Yang, K., Browne, P. R. L., Huntington, J. F., & Walshe, J. L. (2001). Characterising the hydrothermal alteration of the Broadlands-Ohaaki geothermal system, New Zealand, using short-wave infrared spectroscopy. *Journal of Volcanology and Geothermal Research*, *106*(1–2), 53–65. https://doi.org/10.1016/S0377-0273(00)00264-X

Yang, K., Huntington, J. F., Gemmell, J. B., & Scott, K. M. (2011). Variations in composition and abundance of white mica in the hydrothermal alteration system at Hellyer , Tasmania , as revealed by infrared reflectance spectroscopy. *Journal of Geochemical Exploration*, *108*(2), 143–156. https://doi.org/10.1016/j.gexplo.2011.01.001

Zaini, N., van der Meer, F., & van der Werff, H. (2014). Determination of carbonate rock chemistry using laboratory-based hyperspectral imagery. *Remote Sensing*, *6*(5). https://doi.org/10.3390/rs6054149